OPTOELECTRONICS AND ADVANCED MATERIALS – RAPID COMMUNICATIONS Vol. 3, No. 12, December 2009, p. 1383 - 1387

Optical and EPR investigations of the thermal treatment effects on YVO_4 nanocrystals

S. GEORGESCU[*], E. COTOI, A. M. VOICULESCU, O. TOMA, M. N. GRECU[a], E. BORCA[b], S. HODOROGEA[c]
National Institute for Laser, Plasma and Radiation Physics, Magurele, Romania,
[a]*National Institute for Materials Physics, Magurele, Romania*
[b]*Faculty of Physics, Bucharest University, Romania*
[c]*ICPE-CA, Bucharest, Romania*

YVO_4 nanocrystals doped with Eu (5 at.%) or Gd (1 at.%) were synthesized by precipitation method and annealed at various temperatures between 60ºC and 900ºC. The average size (coherence domain) of the YVO_4 and nanocrystals, estimated from X-ray diffraction measurements, varies from ~7 nm to ~60 nm, function of the annealing temperature. The morphological transformations produced by thermal treatments in YVO_4 nanocrystals were monitored using optical spectroscopy with Eu^{3+} as probe and EPR spectroscopy, the paramagnetic probe being Gd^{3+}.

(Received November 24, 2009; accepted November 26, 2009)

Keywords: YVO_4, Eu^{3+}, Gd^{3+}, Nanocrystals, Fluorescence, EPR, Optical spectroscopy

1. Introduction

YVO_4:Eu^{3+} is used as a red phosphor in color television cathode ray tube displays and high pressure mercury lamps. Recent studies show that nanosized YVO_4:Eu has significant promise in plasma display panels (PDP) [1].

Various methods have been used to prepare YVO_4:Eu^{3+} since it was introduced by Levine and Pallia in 1964 [2], high temperature solid state method [3], hydrolyzed colloid reaction technique [4], hydrothermal methods [1,5], precipitation techniques [6,7], flux [8], etc.

YVO_4 has the zircon structure (space group $I4_1/amd$, lattice parameters a = 7.1183 Å, c = 6.2893 Å [9]). The lanthanide ion substitutes yttrium in the YVO_4 lattice. This site has D_{2d} symmetry.

For nanocrystals doped with rare earth ions a valuable tool in the investigation of the morphology changes produced by various thermal treatments is the optical spectroscopy. In the case of Eu^{3+}, the luminescence line spectrum is relatively easy to analyze since the strongest transitions originate from a nondegenerate energy state ($^5D_0$). The magnetic-dipole transition $^5D_0 \rightarrow {}^7F_1$ is a parity allowed transition, practically insensitive to the changes in the Eu^{3+} neighborhood and can be used as an internal standard. On the contrary, the electric-dipole transition $^5D_0 \rightarrow {}^7F_2$ is very sensitive to any changes near Eu^{3+} ion. The asymmetry ratio was defined as the ratio of the areas of electric-dipole $^5D_0 \rightarrow {}^7F_2$ and magnetic-dipole transitions [10]. Consequently, the Eu^{3+} ion has been extensively used to probe the local environment of dopant sites. Very successful was the utilization of Eu^{3+} as probe for structure and dynamics of glasses [10-12].

Though the EPR spectroscopy is very sensitive to the changes in the neighborhood of the paramagnetic ion, this technique was less used in the study of the dielectric nanocrystals doped with rare earth ions. In particular, though Gd^{3+} was used as paramagnetic probe in single crystals or powders of materials with zircon structure [13-15], it was not used in the study of YVO_4 nanocrystals. Gd^{3+} ion is very sensitive to crystal field symmetry and intensity, being appropriate for studying its homogeneity [16-18].

In this paper we use fluorescence spectroscopy (probe Eu^{3+}) and explore the possibilities of EPR spectroscopy with Gd^{3+} as probe to monitor the morphological transformations induced by the thermal treatments in YVO_4 nanocrystals synthesized by direct precipitation reaction. For fluorescence spectroscopy, the parameters chosen for the monitoring of the morphological transformations of YVO_4 are the linewidths of the $^5D_0 \rightarrow {}^7F_1$ emission lines of Eu^{3+}, the integral luminescence and the asymmetry ratio [10]. For EPR spectroscopy, the chosen parameter is the EPR signal intensity (obtained by the double integration of the EPR spectra, normalized to the sample mass).

2. Experimental

YVO_4 nanocrystals were prepared by direct precipitation reaction [6]. Two solutions, $Y(NO_3)_3$ and $Eu(NO_3)_3$ (or $Gd(NO_3)_3$), were prepared and added to a solution of NH_4VO_3 adjusted to pH 12.5 with NaOH. The obtained colloid was heated at 60°C for one hour with magnetic stirring. The resulting nanocrystals of

$YVO_4:Eu^{3+}$ (5 at.%) and $YVO_4:Gd^{3+}$ (1 at.%) were separated from the solution by filtering and then dried at 60°C. The nanopowders were annealed in air, at various temperatures between 300°C and 900°C, for 4 hours.

XRD measurements were performed on a Bruker-AXS diffractometer D8-ADVANCE using Cu Kα radiation.

The experimental apparatus used for optical fluorescence measurements consisted of a 1-m Jarrell-Ash monochromator equipped with an S-20 photomultiplier and a SR 830 lock-in amplifier on line with a computer. Eu^{3+} fluorescence was excited with a Xenon lamp equipped with suitable optical filters (pump transition: $^7F_0 \rightarrow {}^5L_6$).

A JEOL (upgraded JES-ME) X-band EPR spectrometer was used to record EPR spectra of $YVO_4:Gd^{3+}$ nanopowders. The magnetic field was calibrated with DPPH standard marker (g = 2.0036) and the microwave frequency was measured using a digital Pendulum CNT-90 frequency counter.

All the measurements were performed at room temperature.

3. Results

3.1 X-ray diffraction

Regardless the dopant (Eu^{3+} or Gd^{3+}), the XRD patterns showed the same evolution of the crystalline structure of YVO_4 powders during the annealing process. In Fig. 1 are given the diffraction patterns of YVO_4:Eu nanopowders annealed at various temperatures together with the diffraction pattern of the 'as-prepared' (heated at 60°C) sample. The positions of the diffraction lines given in JCPDS#17-341 card are shown as reference in the bottom. Only the XRD lines corresponding to the YVO_4 phase are present, regardless the treatment temperature. The full width at half maximum is determined by the profile fitting procedure, using a Lorentz line shape. The integral widths of diffraction peaks are used in a Williamson-Hall analysis. The resulting apparent crystallite size (coherently scattering domains), $\langle D \rangle_V$, is given in Fig. 2.

We observe three temperature domains in Fig. 2. In the first domain (between 60°C and ~400°C) the size of the particle increases slowly; in the second (~400°C-700°C) a rapid size increase is observed; in the third one (700°C-900°C) no further increase of the particle size is present.

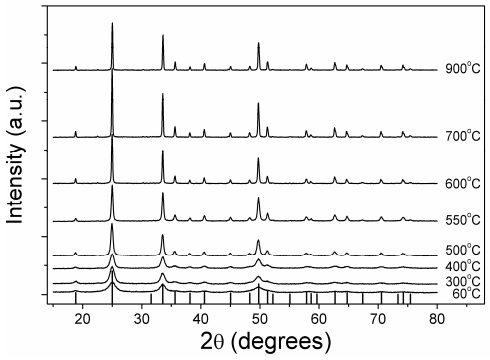

Fig. 1. XRD patterns of YVO_4 powders annealed at various temperatures. The positions of the diffraction lines given in JCPDS#17-341 card are shown as reference in the bottom.

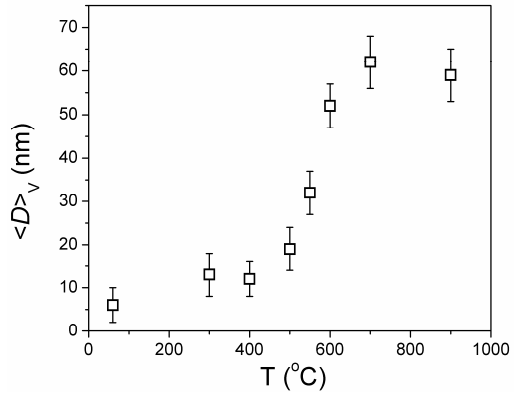

Fig. 2. Effect of annealing temperature on the crystallite size.

3.2 Fluorescence spectra

In Fig. 3 are given the fluorescence spectra (transitions $^5D_0 \rightarrow {}^7F_1$, $^7F_2$, $^7F_3$, $^7F_4$) for two samples of YVO_4:Eu powders: the sample annealed at 900°C and the 'as-prepared' one. The $^5D_0 \rightarrow {}^7F_0$ transition is forbidden in D_{2d} symmetry. The fluorescence spectrum of the sample annealed at 900°C shows much narrower lines and the transitions are better resolved.

The narrowing of the two fluorescence lines of the transition $^5D_0 \rightarrow {}^7F_1$ as a result of the thermal treatment is shown in Fig. 4. These lines are not separated in the spectrum of the 'as-prepared' sample (Fig. 3); therefore, this sample was not considered in Fig. 4. The linewidth decreases rapidly for annealing temperatures between 300°C and 500°C, less rapidly between 500°C and 600°C and remains practically constant for higher temperatures.

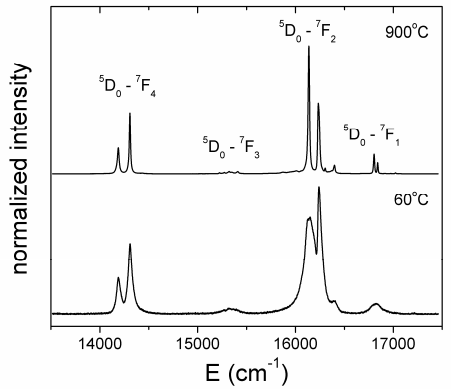

Fig. 3. The fluorescence spectra (transitions $^5D_0 \rightarrow {}^7F_1$, $^7F_2$, $^7F_3$, $^7F_4$) for two samples of YVO_4:Eu powders: the sample annealed at 900°C and the 'as-prepared' one (heated at 60°C).

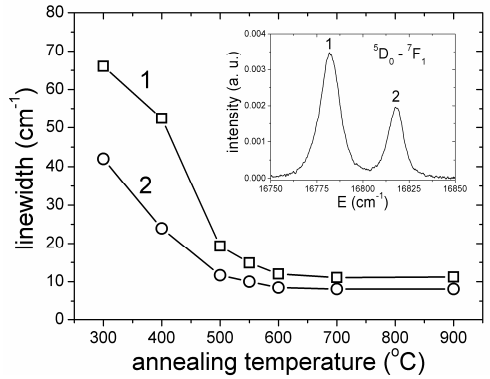

Fig. 4. Dependence linewidth – annealing temperature (transition $^5D_0 \rightarrow {}^7F_1$). Inset: transition $^5D_0 \rightarrow {}^7F_1$.

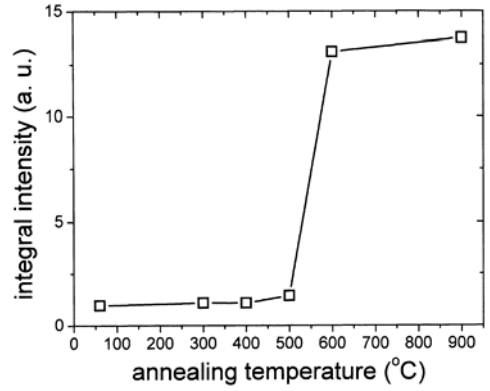

Fig. 5. Integral luminescence as a function of the annealing temperature.

As a measure of the emission efficiency, we measured the integrated luminescence (the area under the luminescence spectra between 13500 and 17500 cm^{-1}) function of the thermal treatment temperature. The result is shown in Fig. 5. Three temperature domains can be delimited: 60°C-500°C, 500°C-600°C and 600°C-higher temperatures.

The asymmetry ratio, defined as

$$R_2 = \frac{Area\left({}^5D_0 \rightarrow {}^7F_2\right)}{Area\left({}^5D_0 \rightarrow {}^7F_1\right)} \quad (1)$$

was estimated from the fluorescence spectra of YVO_4:Eu powders annealed at various temperatures. The results are given in Fig. 6.

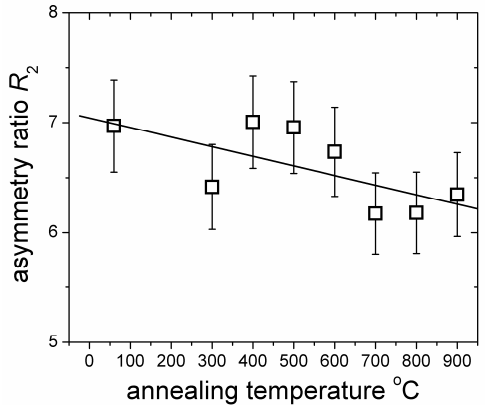

Fig. 6. Asymmetry ratio R_2 as a function of the annealing temperature. The straight line merely suggests t he reduction of R_2 with increasing annealing temperature.

3.3 EPR measurements

The EPR spectra measured for YVO_4:Gd nanopowders annealed at the same temperatures as the YVO_4:Eu ones are given in Fig. 7. The 'as-prepared' sample was further heated at 100°C in order to remove the water traces.

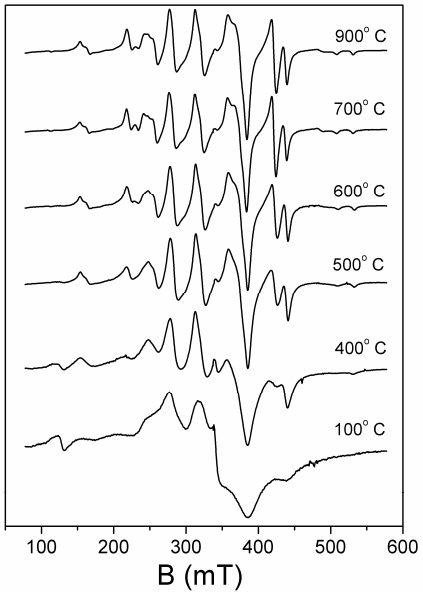

Fig. 7. EPR spectra of YVO_4:Gd nanopowders function of the annealing temperature.

The EPR signal intensity (obtained by the double integration of the EPR spectra, normalized to the sample mass) is shown in Fig. 8. The dependence of the EPR signal follows approximately the dependence of crystallite size (Fig. 2) and of the integral luminescence (Fig. 5).

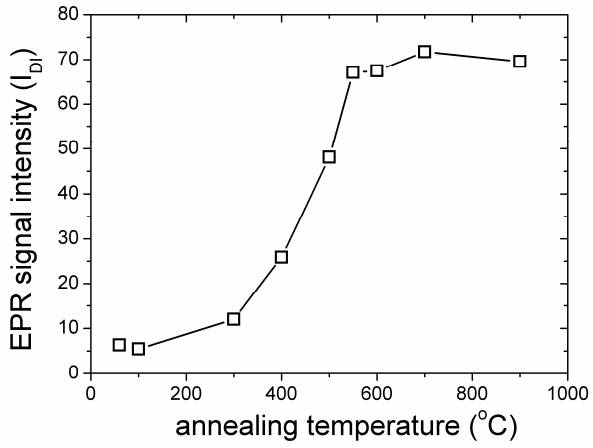

Fig. 7. The intensity of the EPR signal (double integration) as a function of the annealing temperature.

4. Discussion

All the techniques used to monitor the changes produced in the YVO_4 nanocrystals (XRD, optical and EPR spectroscopy) put in evidence approximately the same temperature domains of thermal treatments: (i) 60°C-500°C, (ii) 500°C-600°C, and (iii) 600°C-900°C. In the first domain we note a slow increase of the crystallite size, a very slow increase of the emission efficiency, a slow increase of the EPR signal intensity but a rapid narrowing of the linewidth of the fluorescence lines. In the second temperature interval, the crystallites grow very rapidly; the same behavior is observed for the integral luminescence intensity and the EPR signal intensity; the width of the fluorescence lines decreases with a lower speed. Finally, for temperatures higher than 600°C all the monitored parameters (crystallite size, integral luminescence intensity, fluorescence linewidth, and the EPR signal intensity) remain practically constant. We note that, due to the poor signal / noise ratio, a different behavior of R_2 in the three temperature domain cannot be observed.

We can consider the particle as composed from two parts: the inner part (core), more ordered and the perturbed, less ordered layer near surface. As a result of the increasing of the thermal treatment temperature, the ratio volume / surface increases improving the order, and the impurities (OH^-, NO_3^-, etc.) adsorbed at the particle surface during the wet synthesis are progressively removed. Therefore, the number of the dopant ions (Eu^{3+}, Gd^{3+}) in the particle volume increases in rapport with the number of ions near surface.

The improving order results in the narrowing of fluorescence (Figs. 3, 4) and EPR (Fig. 7) lines.

The electric-dipole transition $^5D_0 \rightarrow {}^7F_1$ is parity forbidden and its probability vanishes for sites possessing inversion symmetry. The probability of this transition increases as the local symmetry is farther from inversion and, generally, a lower value of the asymmetry ratio R_2 for higher local symmetry is expected. Therefore, beside the narrowing of the fluorescence and EPR lines, the improved order should be accompanied with the reduction of R_2, denoting an increase of the local symmetry at Eu^{3+} site (D_{2d} is the 'ideal' symmetry in the bulk material). This behavior is indeed observed in Fig. 6.

We noted that the dependence of the integral intensity of luminescence as well as the EPR signal intensity on the annealing temperature (Figs. 5, 7) follows approximately the dependence of crystallite size (Fig. 2).

The luminescence intensity of Eu^{3+} could be influenced by two main factors: the radiative transition probability and the luminescence quenching by the surface impurities. Longer lifetimes measured for YVO_4:Eu nanoparticles could indicate a lower oscillator strength than in bulk material, which is probably related to the structural disorder induced by the large surface area of the nanoparticles [19]. Therefore, with the increasing particle size, the relative number of Eu^{3+} ions with lower oscillator strength decreases; on the other hand, the number of quenching surface impurities decreases due to the increase of temperature.

Regarding the intensity of EPR signal, we can suppose that the disordered surface makes the resonances of Gd^{3+} ions spread over a large field range, not contributing to the EPR signal. Only the Gd^{3+} ions from the particle volume contribute to the EPR signal and the integral EPR signal intensity follows the temperature dependence observed for the crystallite size.

5. Conclusions

Using the direct precipitation method, YVO_4 nanoparticles (doped with europium or gadolinium) with approximately 7 nm size were synthesized.

In order to monitor the morphologic modifications produced by thermal treatments XRD, optical (probe Eu^{3+}) and EPR spectroscopy (probe Gd^{3+}) were used.

As a result of the thermal treatments (between 300°C and 900°C) the crystallite size increases up to ~ 60 nm. Both optical and EPR spectroscopy gave a similar result: narrowing of the lines (fluorescence, respectively, resonance) and increasing the integral signals (integral fluorescence, integral EPR signal intensity). The increasing of the integral signals follows the temperature dependence of the crystallite size.

The observed facts could be explained by the increasing of the core / surface ratio of the YVO_4 particles and the improvement of the order as a result of the thermal treatments.

Acknowledgements

This work was supported by the project 12089/2008 (INFODOT) of the National Center for Management of Programs of the Romanian Ministry of Education, Research and Innovation, in the frame of the Program 4.

References

[1] K. Riwotzki, M. Haase, J. Phys. Chem. B **102**, 10129 (1998).
[2] A. K. Levine, F. C. Palilla, Appl. Phys. Lett. **5**, 118 (1964).
[3] R. C. Ropp, J. Electrochem. Soc. **115**, 940 (1968).
[4] S. Erdei, J. Mater. Sci. **30**, 4950 (1995).
[5] H. Wu, H. Xu, Q. Su, T. Chen, M. Wu, J. Mater. Chem. **13**, 1223 (2003).
[6] Y. Li, G. Hong, J. Sol. State Chem., **178**, 645 (2005).
[7] A. Newport, J. Silver, A. Vecht, J. Electrochem. Soc. **147**, 3944 (2000).
[8] S. Erdei, J. Crystal Growth, **134**, 1 (1993).
[9] B. C. Chakoumakos, M. M. Abraham, L. A. Boatner, J. Solid State Chem. **109**, 197 (1994).
[10] R. Reisfeld, E. Zigansky, M. Gaft, Mol. Phys. **102**, 1319 (2004).
[11] T. Kushida, Journal of Luminescence **100**, 73 (2002).
[12] C. Brecher, L. A. Riseberg, Phys. Rev. B **21**, 2607 (1980).
[13] J. Rosenthal, Phys. Rev. **164**, 363 (1967).
[14] J. Rosenthal, R. F. Riley, U. Ranon, Phys. Rev. **177**, 625 (1969).
[15] R. W. Reynolds, L. A Boatner, C. B. Finch, A. Chatelain, M. M. Abraham, J. Chem. Phys., **56**, 5607 (1972).
[16] M. Rappaz, L. A. Boatner, M. M. Abraham, J. Chem. Phys. **73**, 1095 (1980).
[17] J. Y. Buzaré, M Fayet-Bonnel, J. C. Fayet, J. Phys. C: Solid State Phys., **14,** 67 (1981).
[18] V. Simon, R. V. F. Turcu, D. Eniu, S. Simon, Physica B **403**, 139 (2008).
[19] A. Huignard, V. Buissette, G. Laurent, T. Gacoin, J.-P. Boilot, Chem. Mater. **14**, 2264 (2002).

*Corresponding author: serban.georgescu@inflpr.ro